In-phase Supermode Operation in Ring Coherent VCSEL Arrays with a Fractional Talbot Cavity

Wei Li, Jing Jing Dai*, Sheng Nan Li, Dong Yue Jin, and Zhi Yong Wang*

*Correspondence to: daijingjing@bjut.edu.cn; zywang@bjut.edu.cn

Abstract—**In-phase coherent vertical cavity surface emitting laser (VCSEL) arrays have desirable properties for high-brightness laser applications. We employ mutual injection feedback modeling of ring VCSEL arrays with fractional Talbot cavity to select their supermodes. An analysis of the effects of Talbot cavity lengths on engineering the coupling coefficient and gain threshold for in-phase mode operation is provided through the overlapping integrals of optical field distributions. An example design for 24-element arrays with a fractional Talbot cavity is presented, and the in-phase far-field distribution is obtained. This provides a potential method for fabricating Bessel Gaussian beams using larger ring VCSEL arrays.**

Index Terms—**Coherent array, in-phase mode, fractional Talbot cavity, vertical-cavity surface-emitting laser (VCSEL).**

I. INTRODUCTION

VERTICAL cavity surface emitting lasers (VCSELs) enable easy realization of 2D integration to achieve high output power[1-4]. Because of their inherent excellent characteristics, VCSELs are potential in many fields, such as laser communication[5], laser radar[6-7], 3D sensing[8], light detection and ranging[9] in recent years. However, individual VCSEL are operated independently in such 2D arrays, which leads to a decrease in coherence and an increase in far-field divergence angle. Coherent VCSEL arrays have been previously explored for the generation of diffraction-limited or high brightness beams[10]. When coherently coupled, optical coupling and mutual injection locking are performed among the elements[11]. Thus, VCSEL arrays can operate in a single coherent supermode which can be classified as the out-of-phase (the phase difference between adjacent elements is π) or in-phase (the phase difference between adjacent elements is 0) supermode, respectively[12-13]. The power of in-phase mode will concentrate on the central lobe to obtain on-axis maximum, while the out-of-

phase mode results in far-field null on axis[14-16]. Obviously, the in-phase mode will be more preferred in many applications[17].

Several different designs have been proposed to achieve phase-locked of VCSEL elements[18-20]. Diffraction coupling by an external cavity is a practical approach based on Fresnel diffraction theory[21-23]. Phase locking is achieved by the injection of the external optical feedback into the inner cavity of VCSELs[24-26]. But out-of-phase mode can be induced by external cavity. In addition, Nusrat Jahan et al[14] demonstrated anti-guided triangular photonic crystal VCSEL arrays, which produced high-brightness in-phase mode lasers. However, this approach requires strict design and a complex fabrication process for the photonic crystal. Another feasible mean of optical coupling between VCSEL elements is proton implantation. Xun meng et al[27-28] fabricated implant-defined various VCSEL arrays. The proton implantation procedure is considerably simple, but it can injure the epitaxial structure, which is not conducive to the stability of the device.

Talbot cavity is a method of obtaining efficient mutual injection by parallel coupling to achieve in-phase mode lasing[11,29]. In this work, building on the Talbot effect of the ring laser array and past numerical simulations[30], we propose employing the diffraction coupling effect of the Talbot cavity to obtain in-phase mode operation of ring VCSEL arrays. Lasing supermodes, whether in-phase mode or out-of-phase mode, are characterized by a coupling coefficient that quantifies the coupling among the optical fields. The coupling coefficient is calculated using the overlapping integrals of optical field distribution at fractional Talbot planes. Supermode analysis of arrays in Talbot cavity has linked the coupling coefficients to the difference in the optical field distribution of the in-phase and out-of phase modes. We extend our analysis to a 940 nm 24-elements ring VCSEL arrays with a fractional Talbot cavity and demonstrate that the lasing supermode operates in the in-phase mode at a cavity length of Zt/8. This external cavity structure is also applicable to other 2-D VCSEL arrays. Furthermore, We prove that the in-phase mode ring VCSEL arrays should generate Bessel Gaussian beams with low beam divergence in theory.

II. PRINCIPLES

A. Design of the Fractional Talbot Cavity Setup

As shown in Fig. 1(a), we employ a top-emitting VCSEL and a fractional Talbot cavity to construct the ring VCSEL array model. The light from the emitting apertures is reflected

by the fractional Talbot cavity and injected back into the ring arrays, forming optical feedback. The emitting apertures are defined by mesa etching. The microscope image of the ring arrays with a radius of 100 μm is shown in Fig. 1(d), which is composed of 24 elements. What distinguishes it from a typical self-lasing device is that the VCSEL has only partial P-DBR, as shown in Fig. 1(c); consequently, its reflectivity is not high enough to lase by itself. We provide additional reflectivity by coating λ/4 films on an adjustable length external cavity, as shown in Fig. 1(b). Aiming at the injection feedback problem in fractional Talbot cavity, accurate analysis of the supermode field and determination of the effect of optical field coupling on supermode selection are necessary.
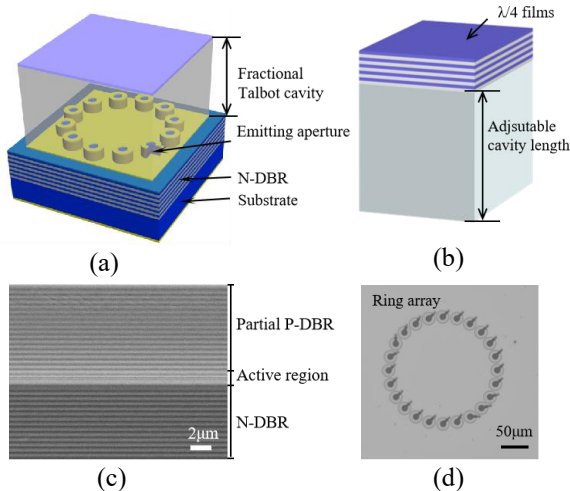

(a) (b)

(c) (d)

Fig. 1. (a) Schematic of the ring VCSEL arrays; (b) schematic of the fractional Talbot cavity; (c) scanning electron microscope image of the VCSEL chip; (d) microscope image of the emitting apertures.

B. Analysis of Supermode Field

The supermode selection is explained by the theory of Talbot images at fractional Talbot planes and achieved through injection locking. That is, the phase difference is becoming constant by using the mutual injection between different elements. Re-images by the Talbot effect is used as the optical feedback for the mutual injection locking of the VCSEL arrays by placing an output coupling mirror at fractional Talbot distance. The field distribution of different supermodes leads to mode selectivity in fractional Talbot cavity.

The Talbot effect is derived by the calculation of Fresnel-Kirchhoff integration with an infinitely periodic structure[31]. The diffraction image exhibiting the same periodical pattern as the original is re-imaged at the Talbot distance which is calculated as below[30]

$$Zt = \frac{2np^2}{\lambda} \tag{1}$$

where Zt is the Talbot distance, p is the period of the array, n is an integer and λ is the wavelength. The ring arrays, which are constituted by patterns with a period $p = r_0 \theta_0$, can be regarded as periodic infinite elements in the angular direction. r_0 is the

radius of the ring arrays, and θ_0 is the central angle between two adjacent elements.

It has been found that external cavity feedback induces VCSEL arrays to lase in either the lowest or highest order supermode. These two modes correspond to in-phase mode and out-of-phase mode, respectively[15]. At fractional Talbot planes, arrays of in-phase and out-of-phase modes will form a series of re-images, respectively. In Fig. 2(a) and 3(a), we display the transverse intensity distribution of in-phase and out-of-phase mode at different fractional Talbot planes (the radius of arrays r_0 = 100 μm). The fractional Talbot image of in-phase mode at Zt/2 exhibits a p/2 shift compared to the array arrangement, while for the Zt/4 fractional Talbot image, the transverse period is halved. Meanwhile, the fractional Talbot image of out-of-phase mode at Zt/4 exhibits a p/4 period shift compared to the array arrangement, and the transverse period is also halved. Fig. 2(b) and 3(b) illustrate the Talbot carpets of in-phase and out-of-phase modes, clearly showing the spatial shift and variation in the number of spots in the angular direction at fractional Talbot planes.
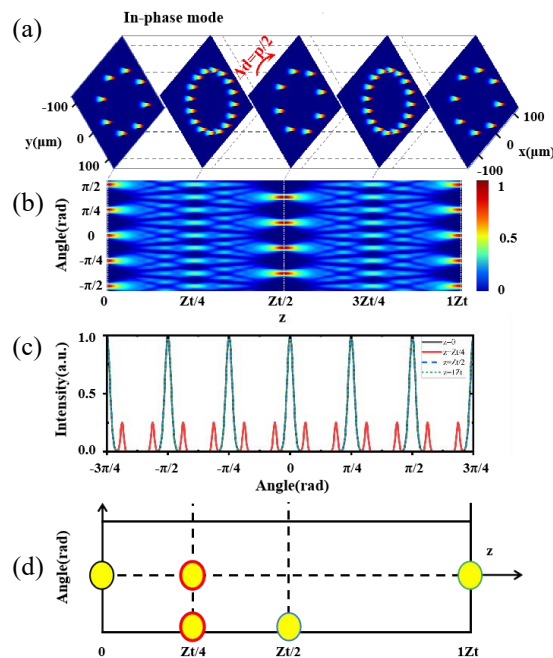

Fig. 2. The Talbot images of in-phase mode. (a) The fractional Talbot images of at fractional Talbot planes; (b) the Talbot carpet; (c) the transverse intensity distribution; (d) the spatial shift of in-phase mode.
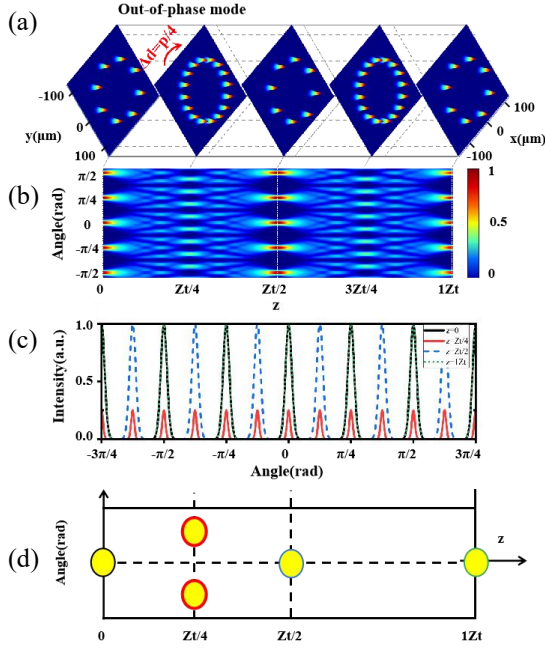
Fig. 3. The Talbot images of out-of-phase mode. (a) The fractional Talbot images of at fractional Talbot planes; (b) the Talbot carpet; (c) the transverse intensity distribution; (d) the spatial shift of out-of-phase mode.

In Fig. 2(c) and 3(c), the intensity distributions at along the angle θ axes z = 0, z = Zt/4, z = Zt/2, and z = 1Zt are displayed. Due to the doubling of the number of re-images, the intensity of the spots at the Zt/4 plane is 1/4 of the emitted intensity. Besides, it is clear that the spatial distribution of re-images of in-phase and out-of-phase mode is different at fractional Talbot planes in Fig. 2(d) and 3(d). The out-of-phase mode exhibits self-images at both the Zt/2 and 1Zt planes, but the period shift at the Zt/4 plane, which provides a possibility to suppress the injection of the out-of-phase mode. Hence, we can examine the influence of cavity length L on the field distribution of feedback light, which distinguishes the light injection efficiency between in-phase and out-of-phase modes.

C. In-phase Mode Selection

The Talbot image provides light injection feedback to change the gain thresholds of supermodes, which is linked via a coupling coefficient, C_m. By effectively coupling into the laser gain region, the VCSEL can operate in in-phase mode eventually. According to the coupled mode theory, the coupling strength between the array elements can be quantified using the coupling coefficient C_m which is expressed as[25,32]

$$C_m = \frac{\int_{r=0}^{r=\omega_0} \int_{\theta=-\pi}^{\theta=\pi} E_{tol}^*(r,\theta,2z) \cdot E_m(r,\theta,0) r dr d\theta}{\left(\int_{r=0}^{r=\omega_0} \int_{\theta=-\pi}^{\theta=\pi} |E_{tol}(r,\theta,2z)|^2 r dr d\theta\right)^{1/2} \cdot \left(\int_{r=0}^{r=\omega_0} \int_{\theta=-\pi}^{\theta=\pi} |E_m(r,\theta,0)|^2 r dr d\theta\right)^{1/2}} \quad (2)$$

where $E_{tol}(r,\theta,2z)$ is the superposed field distribution after round-trip transmission of all elements through the Talbot cavity, $E_m(r,\theta,0)$ is the intensity distribution of the element m in the initial plane and $E_{tol}^*(r,\theta,2z)$ is the complex conjugate of $E_{tol}(r,\theta,2z)$. C_m denotes the coupling field overlap of the superposed field distribution of all elements over the cross-sectional area of element m. We calculate the oscillating curves of coupling coefficients of in-phase and out-of-phase modes in fractional Talbot cavities, as shown in Fig 4(a). The i and ii points indicate that when cavity length L = Zt/8, the difference in coupling coefficients between in-phase and out-of-phase modes is the largest. At this cavity length, the in-phase mode achieves higher optical feedback.

The VCSEL arrays with a Talbot cavity can be equivalent to a composite resonator, and the equivalent reflectivity R_{eff} which is shown in Fig. 4(b) is described as follows[1]

$$R_{eff} = \left[\sqrt{R_2} + \frac{(1-R_2)\sqrt{R_e}}{1+\sqrt{R_2 R_e}}\right]^2 \quad (3)$$

where R_2 is the reflectivity of the P-DBR and R_e is the reflectivity of the output coupling mirror. According to the self-reproduction condition of VCSEL, combined with the influences of the light injection from Talbot re-images, the amplitude self-reproduction condition can be obtained[33]

$$R_1 R_{eff} C_m \exp\left[2\Gamma(g_{th} - \alpha_{int})d - 2\alpha_m(l-d)\right] = 1 \quad (4)$$

where R_1 is the reflectivity of N-DBR, l is the length of the inner cavity, d is the thickness of the active layer, Γ is the confinement factor, α_m is the mirror loss and α_{int} is the inner cavity loss. The gain threshold g_{th} is obtained as

$$g_{th} = \alpha_{int} + \frac{1}{\Gamma d}\left[\alpha_m(l-d) + \ln\frac{1}{\sqrt{R_1 R_{eff} C_m}}\right] \quad (5)$$

Table 1 presents typical parameters used for this analysis. In Fig. 4(a), we display the variation curves of gain threshold for in-phase and out-of-phase modes with cavity length, as well as the relationship curve between gain threshold and coupling coefficient within a range of 1Zt, respectively. The insets in Fig. 4(a) show the threshold of the in-phase mode at point i is lower than that of the out-of-phase mode at point ii, at which we select the in-phase mode lasing when the cavity length is Zt/8. The insets in Fig. 4(c) show the far-field distribution of in-phase and out-of-phase modes. The far-field energy of in-phase mode is concentrated on the axial main lobe, while that of the out-of-phase mode is dispersed in the annular secondary side lobes.

TABLE 1
PARAMETERS USED IN THE SIMULATION

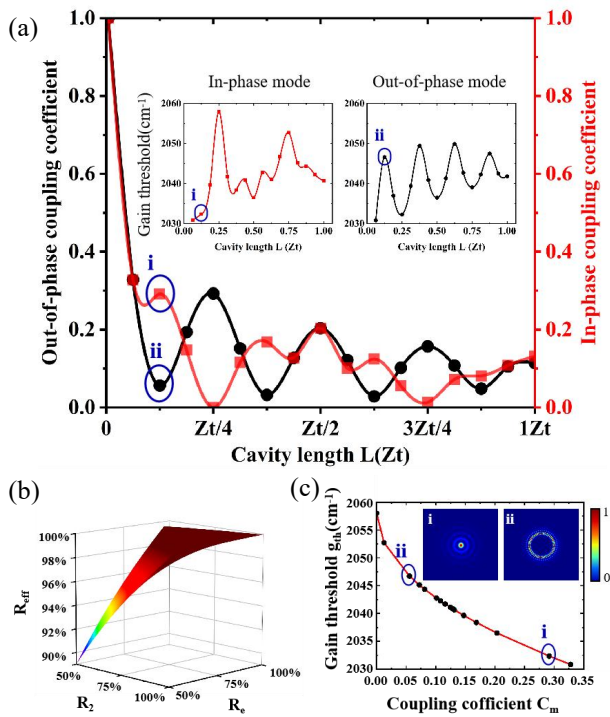| Symbol	Quantity	Value	Unit
l	inner cavity length	7	μm
R_1	the reflectivity of N-DBR	0.9998	-
R_2	the reflectivity of P-DBR	0.94	-
R_e	the reflectivity of mirror	0.80	-
α_{int}	inner cavity loss	2000	cm⁻¹
α_m	mirror loss	1.16×10^5	cm⁻¹
Γ	confinement factor	0.05	-
d	Active layer thickness	0.3	μm

Fig. 4. (a) Calculated coupling coefficients of the in-phase (red line) and out-of-phase (black line) supermodes as a function of cavity length L. The insets show gain thresholds of the in-phase (red line) and out-of-phase (black line) supermodes; (b) the composite reflectivity composed of P-DBR and output coupling mirror; (c) the influence of coupling coefficient on supermode gain threshold. The insets show the normalized far-field intensity at points (i) and (ii).

III. EXPERIMENT AND ANALYSIS

We fabricated top-emitting VCSEL chip designed for emission around 940nm. The top distributed Bragg reflector (DBR) consists of 11 pairs of p-doped $Al_{0.035}Ga_{0.965}As$–$Al_{0.86}Ga_{0.14}As$ quarter wavelength layers. The bottom DBRs consists of 41 pairs of the same composition layers of n-type. 1 junction roughly 300 nm-thick with 3 pairs of $GaAs/Al_{0.3}Ga_{0.7}As$ quantum wells is sandwiched between P-DBR and N-DBR. A 20 nm-thick $Al_{0.98}Ga_{0.02}As$ layer is centered on the interface between the quantum wells and the PDBR layers. The ring VCSEL array elements are defined by mesa etching and wet oxidation. The fabrication process is as follows. First, a 500 nm-thick SiO_2 layer was deposited on the chip surface and mesas are generated by inductively coupled plasma (ICP) etching on the chip surface. Then, controlling oxidation depth by wet oxidation technology to achieve electrical isolation and light confinement, and an oxidation aperture with a diameter of 7 μm is formed. Finally, Ti/Pt/Au and Ni/Ge/Au metal layers are sequentially deposited to form P and N electrodes by UV lithography, electron beam evaporation and metal lift-off techniques. The width of the Ohmic contact electrode is designed for 3 μm to improve current injection uniformity. The Talbot cavity is prepared by coating films on a quartz with a thickness of 273 μm, which is mirror-polished by Chemical Mechanical Polishing (CMP) to reduce scattering losses and bonded onto the chip.

Fig. 5(a) shows the microscopic image of near field for 24-elements ring arrays under 50 mA. In the Talbot cavity, the standing wave field emitted by the arrays maintains a ring field distribution. Fig 5(b) shows a a characteristic of output power versus injection current for 24-elements ring arrays under QCW conditions (500 μs on, 10% duty). The maximum output power for the 24-elements VCSEL arrays is 17 mW. And the threshold current is 21 mA for the array. Via Talbot cavity phase locking, the far-field spot becomes a single main lobe. The FWHM of the spectrum is 1.1 nm under 50 mA, and only one peak appears in the spectral lines, showing single longitudinal mode operation in Fig. 5(c). Two flat convex mirrors with a focal length of 100 mm and a distance of 200 mm apart were positioned in front of the CCD to record the near-field distributions. From direct measurement of near field, we can easily observe the Talbot images of in-phase mode at different planes as shown in Fig. 5(d). Move the CCD to the Zt/4 plane and observe compact images with a halved period. As the CCD moves backward, images with the same period but half a period spatial shift, images with double periods, and re-images were observed at the Zt/2, 3Zt/4 and 1Zt planes, respectively.
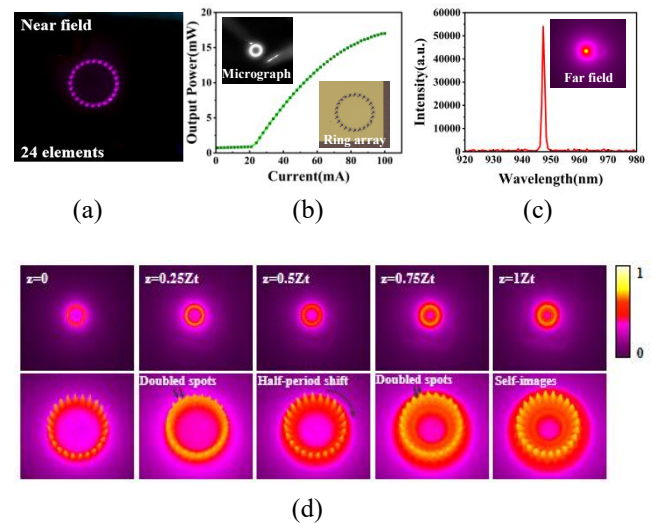

Fig. 5. (a) Near field of 24-elements ring arrays; (b) output power versus injection current of a 24-elements arrays with Talbot cavity under QCW condition; (c) spectra of a 24-elements in-phase mode VCSEL arrays with the Talbot cavity; (d) the Talbot images of in-phase mode at fractional Talbot planes.

We also fabricated 16-elements ring VCSEL arrays with the same ring radius (100 μm) and emitting apertures. The near-field Talbot images were measured using the same method under 50 mA as shown in Fig. 6. It is noted that the increase in cycle makes the generated Talbot images clearer and it still keeps an in-phase mode operation for 16-elements arrays.
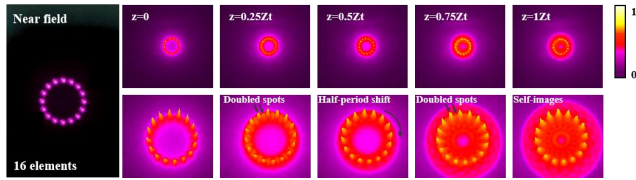
Fig. 6. The Talbot images of 16-elements ring VCSEL arrays at fractional Talbot planes.

To evaluate our research results, we built 3-D coherent array models theoretically to research on the optical field transmission process of ring arrays. In the simulation, the beam emitting from every element was set as Gaussian beam. The initial phase of every Gaussian beam was 0 to form in-phase mode. The Gaussian beam waist radius is 5 μm. The models are set as a 45-elements array with a radius of 250 μm ($r_0 = 250$ μm) and 500 μm ($r_0 = 500$ μm), respectively.

The near field and far field distributions of the two 45-elements array are indicated in Fig. 7. The far field distributions of both exhibit the form of Bessel Gaussian beams with a single main lobe and multiple concentric ring side lobes, which is consistent with the content of previous research[34-35]. From the x-z cross-section, we find the main lobes of two arrays both have a non-diffraction stage. Obviously, the stage in $r_0 = 500$ μm array is approximately twice as long as that in $r_0 = 250$ μm array.

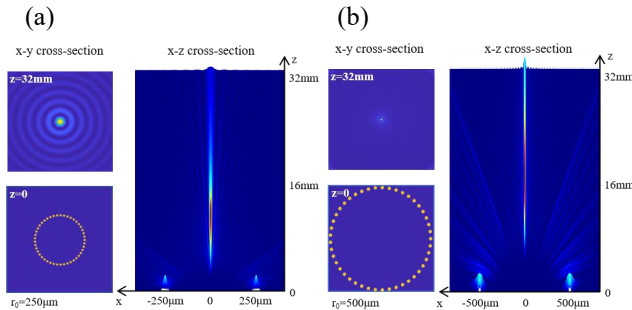**Fig. 7.** Near field and far field distributions of 45-elements arrays with a radius of 250 μm (a) and with a radius of 500 μm (b).

Then, two sets of simulations were conducted to analyze the effects of enlarging the array radius and increasing the number of elements on the far-field distribution. Fig. 8(a) shows the far field distributions of three arrays of $r_0 = 250$ μm with 45-elements, 90-elements and 135-elements at z = 32 mm plane, respectively. It can be observed that increasing the number of elements will only result in an increase in peak intensity, while the widths of the main lobes at each order remain the same. Fig. 8(b) shows the far field distributions of three 45-elements arrays of $r_0 = 250$ μm, $r_0 = 375$ μm and $r_0 = 500$ μm at z = 32 mm plane, respectively. We found that although the peak intensity may slightly decrease, enlarging the array radius effectively reduces the width of the main lobe. Therefore, it is expected to achieve long-distance non-diffraction transmission and obtain small divergence angles by fabricating large-scale ring coherent arrays.
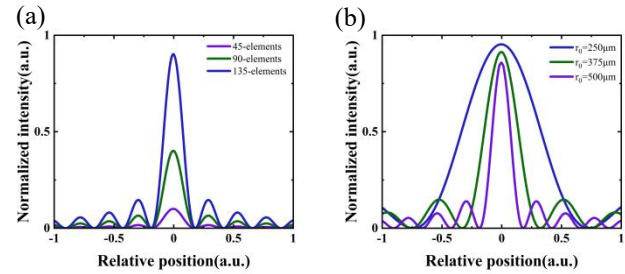

Fig. 8. Simulated far field distributions of large-scale ring arrays at z = 32 mm plane.(a) The far-field distributions of arrays with different radii; (b) the far-field distributions of arrays with different elements.

IV. CONCLUSION

We established a model of a ring VCSEL array with fractional Talbot cavity, and analyzed the supermodes field inside the cavity. By solving the coupling coefficient and gain threshold of the supermodes, we obtained the cavity length for in-phase mode operation. We designed and fabricated a ring VCSEL array device to achieve in-phase mode coherent output with a single main lobe distribution in the far field. Further simulation of the transmission characteristics of large-scale ring arrays shows that a non-diffraction transmission stage is obtained in the far-field of in-phase ring arrays. The experimental results are consistent with a model of the expected in-phase supermode field. Our research has the potential to use ring VCSEL arrays to generate a Bessel-Gaussian beam and apply it to optical communication and optical micro operations.

REFERENCES

[1] D. Zhou, J. F. Seurin, G. Xu, P. Zhao, and C. Ghosh, "Progress on high-power high-brightness VCSELs and applications," presented at the Conference on Vertical-Cavity Surface-Emitting Lasers XIX, San Francisco, CA, USA, 2015.

[2] Q. Yuan, H. Jing, Q. Zhang, L. Zhong, and X. Ma, "Development and Applications of GaAs-Based Near-Infrared High Power Semiconductor Lasers," *Laser Optoelectron. Prog.,* vol. 56, no. 4, p. 040003, 2019. doi:10.3788/LOP56.040003.

[3] K. Iga, "Forty years of vertical-cavity surface-emitting laser: Invention and innovation," *Jpn. J. Appl. Phys.,* vol. 57, no. 8s2, pp. 08PA01.1-08PA01.7, 2018. doi:10.7567/JJAP.57.08PA01.

[4] C. Wang, C. Li, J. Dai, and Z. Wang, "Study on in-chip phase locked high brightness bottom emitting Talbot-VCSELs array," presented at the AOPC 2020: Advanced Laser Technology and Application, Beijing, China, 2020.

[5] J. A. Lott, "Vertical Cavity Surface Emitting Laser Diodes for Communication, Sensing, and Integration," in *Semiconductor Nanophotonics*, vol. 194. Switzerland: Springer: Cham, 2020, pp. 391-424.

[6] S. Kakuma, "Frequency-modulated continuous-wave laser radar using dual vertical-cavity surface-emitting laser diodes for real-time measurements of distance and radial velocity," *Opt. Rev.,* vol. 24, no. 1, pp. 39-46, 2017. doi:10.1007/s10043-016-0294-7.

[7] Y. Han, Z. Li, L. Wu, S. Mai, X. Xing, and H. Fu, "High-Speed Two-Dimensional Spectral-Scanning Coherent LiDAR System Based on Tunable VCSEL," *J. Lightwave Technol.,* vol. 41, no. 2, pp. 412-419, 2023. doi:10.1109/JLT.2022.3217088.

[8] Ebeling *et al.*, "Vertical-cavity surface-emitting laser technology applications with focus on sensors and three-dimensional

imaging," *Jpn. J. Appl. Phys.,* vol. 57, no. 8, 2018. doi:10.7567/JJAP.57.08PA02.

[9] J. Zhang *et al.*, "910 nm vertical-cavity surface-emitting laser arrays with 100 W output power level and low driving current," *Jpn. J. Appl. Phys,* vol. 57, no. 10, pp. 100302.1-100302.5, 2018. doi:10.7567/JJAP.57.100302.

[10] N. Yokota, K. Ikeda, and H. Yasaka, "Injection-locked spin-VCSELs for coherent optical communications," presented at the Conference on Spintronics XV held as part of SPIE Nanoscience and Engineering Conference, San Diego, CA, USA, 2022.

[11] T. Shichijo and T. Miyamoto, "Rate equation-based numerical analysis of mutual injection for phase locked 2D-VCSEL array using Talbot effect," *Jpn. J. Appl. Phys.,* vol. 58, no. SJ, pp. SJJC01 (9pp), 2019. doi:10.7567/1347-4065/ab1b66.

[12] N. Jahan and K. D. Choquette, "Supermode Analysis and Characterization of Triangular Vertical Cavity Surface Emitting Laser Diode Arrays," *IEEE Photonics J.,* vol. 15, no. 4, p. 1501607, 2023. doi:10.1109/JPHOT.2023.3293427.

[13] G. Pan *et al.*, "Enhancing beam quality and optical intensity of partially coherent VCSEL array by on-chip integrating micro optical phase modulators," *Jpn. J. Appl. Phys.,* vol. 58, no. 8, p. 80905, 2019. doi:10.7567/1347-4065/ab30a9.

[14] N. Jahan, W. North, P. Strzebonski, and K. D. Choquette, "Supermode Switching in Coherently-Coupled Vertical Cavity Surface Emitting Laser Diode Arrays," *IEEE J. Sel. Top. Quantum Electron.,* vol. 28, no. 1, p. 1700505, 2022. doi:10.1109/JSTQE.2021.3117236.

[15] J. R. Leger, "Lateral mode control of an AlGaAs laser array in a Talbot cavity," *Appl. Phys. Lett.,* vol. 55, no. 4, pp. 334-336, 1989. doi:10.1063/1.101900.

[16] E. B. Y. Nair, "Almost perfect in-phase and anti-phase chaotic and periodic phase synchronization in large arrays of diode lasers," *Opt. Commun.,* vol. 430, pp. 104-111, 2019. doi:10.1016/j.optcom.2018.08.020.

[17] M. Kuramoto, S. Kobayashi, K. Tazawa, K. Tanaka, T. Akagi, and T. Saito, "In-phase supermode operation in GaN-based vertical-cavity surface-emitting laser," *Appl. Phys. Lett.,* vol. 115, no. 4, p. 041101, 2019. doi:10.1063/1.5104289.

[18] M. M. M. *et al.*, "High Beam Quality of In-Phase Coherent Coupling 2-D VCSEL Arrays Based on Proton-Implantation," *IEEE Photonics Technol. Lett.,* vol. 26, no. 4, pp. 395-397, 2014. doi:10.1109/LPT.2013.2295101.

[19] D. H. *et al.*, "Enhanced Digital Modulation of Coherent Photonic Crystal VCSEL Arrays," in *2018 IEEE International Semiconductor Laser Conference (ISLC)*, 2018, pp. 1-2, doi: 10.1109/ISLC.2018.8516257.

[20] G. Hergenhan, B. Luecke, and U. Brauch, "Experiments on the scalability of the coherent coupling of VCSEL arrays,", vol. 4649, 2002.

[21] V. P. Kandidov and A. V. Kondrat Ev, "Collective modes of laser arrays in Talbot cavities of various geometries," *Quantum Electron.,* vol. 27, no. 3, p. 234, 1997. doi:10.1070/QE1997v027n03ABEH000909.

[22] V. P. Kandidov and A. V. Kondrat Ev, "Influence of the Talbot cavity selectivity on the evolution of collective operation of diffraction-coupled laser arrays," *Quantum Electron.,* vol. 28, no. 11, p. 972, 1998. doi:10.1070/QE1998v028n11ABEH001367.

[23] V. P. Kandidov, A. V. Kondrat'Ev, and M. B. Surovitskii, "Collective modes of a 2D laser array with diffraction coupling," presented at the 6th International Conference on Industrial Lasers and Laser Applications, Shatura, Moscow Region, Russian Federation, 1999/1/1, 1999.

[24] Liu, Bo, Braiman, and Yehuda, "Coherent addition of high power broad-area laser diodes with a compact VBG V-shaped external Talbot cavity," *Opt. Commun.,* vol. 414, pp. 202-206, 2018. doi:10.1016/j.optcom.2018.01.021.

[25] C. Wen, W. Li, J. Dai, S. Ma, and Z. Wang, "Study on Supermode Control of External Cavity VCSEL Array with Parallel-Coupled Model," *Photonics,* vol. 10, no. 2, p. 115, 2023. doi:10.3390/photonics10020115.

[26] V. I. Kopp, J. Park, J. Singer, N. Dan, and A. Z. Genack, "Lasing modes in a monolithic Talbot cavity," *J. Lightwave Technol.,* vol. PP, no. 99, p. 1-1, 2021.

[27] Meng *et al.*, "Nineteen-element in-phase coherent vertical-cavity surface-emitting laser array with low side lobe intensity," *Opt. Express,* vol. 27, no. 2, pp. 774-782, 2019. doi:10.1364/OE.27.000774.

[28] M. Xun, Y. Sun, X. Jiang, R. Zhang, and J. Zhou, "Stable in-Phase Mode Operation in Coherent VCSEL Array With an Integrated Phase Shifter," *IEEE Trans. Electron Devices,* vol. 67, no. 7, pp. 2819-2824, 2020. doi:10.1109/TED.2020.2994274.

[29] H. F. T. E. S., "I. Facts relating to optical science. No. III," *Philosophical Magazine Series 3,* vol. 9, no. 56, p. 401, 1836. doi:10.1080/14786443608636441.

[30] W. Li, J. Dai, C. Wen, M. Zong, S. Li, and Z. Wang, "Talbot effect of ring laser array realized by Gyrator canonical transformation," *Acta Phys. Sin.,* vol. 72, no. 5, pp. 054208-1-054208-5, 2023. doi:10.7498/aps.72.20222412.

[31] V. P. Kandidov, A. V. Kondrat'Ev, and M. B. Surovitskii, "Collective modes of two-dimensional laser arrays in a Talbot cavity," *Quantum Electron.,* vol. 28, no. 8, p. 692, 1998. doi:10.1070/QE1998v028n08ABEH001220.

[32] Y. Ma *et al.*, "Phase-locking dynamics of a 2D VCSEL hexagonal array with an integrated Talbot cavity," *Opt. Express,* vol. 30, no. 6, pp. 9892-9903, 2022. doi:10.1364/oe.452548.

[33] M. S. Torre and C. Masoller, "VCSEL Fundamentals," in *Fundamentals, Technology and Applications of Vertical-Cavity Surface-Emitting Lasers*, vol. 166. Ulm: Springer Series in Optical Sciences, 2013, pp. 28-30.

[34] Z. Zhi *et al.*, "On-chip generation of Bessel–Gaussian beam via concentrically distributed grating arrays for long-range sensing," *Light: Science & Applications,* vol. 12, no. 1, p. 92, 2023. doi:10.1038/s41377-023-01133-2.

[35] F. Gori, G. Guattari, and C. Padovani, "Bessel-Gauss beams," *Opt. Commun.,* vol. 64, no. 6, pp. 491-495, 1987. doi:https://doi.org/10.1016/0030-4018(87)90276-8.

Wei Li, received the B.Eng. degree in electronic science and technology from Xidian University. He is currently working toward the Ph.D. degree in optics engineering at Beijing University of Technology. His research focuses on semiconductor laser optoelectronic chip and integrated technology. His doctoral thesis is on the research of high-power, high-beam-quality semiconductor lasers.

Jing Jing Dai, received the M.S. and Ph.D. degrees in optical engineering from Beijing University of Technology, Beijing, China, in 2010 and 2022, respectively. She is currently a senior engineer with the School of Physics and Optoelectronic Engineering. Her research interests include high power edge emitting and vertical cavity surface emitting laser chip and space debris detection and feature recognition.

Sheng Nan Li, received the B.Sc. degree in optoelectronic information science and engineering from Hebei University. She is currently working toward the Ph.D. degree in electronic science and technology at Beijing University of Technology. Her research focuses on semiconductor laser optoelectronic chip and integrated technology.

Dong Yue Jin, received the Ph.D. degree in electronic science and technology from Beijing University of Technology, Beijing, China, in 2009. She is currently an associate professor with the School of Electronic Information and Control Engineering, Beijing University of Technology. Her research interests include reliability of radio frequency (RF)/microwave (MW) devices and RF/MW integrated circuits, microelectronic devices and integrated circuits.

Zhi Yong Wang, received the M.S. and Ph.D. degrees in optical engineering from Beijing University of Technology, Beijing, China, in 1995 and 1998, respectively. He is currently a Professor with the School of Physics and Optoelectronic Engineering. He was also the director with Institute of Advanced Technology on Semiconductor Optics & Electronics. His research interests include high power and high beam quality semiconductor laser technology, high brightness semiconductor pump source technology, and high-power fiber laser and its application technology.